Chalcogenide Letters Vol. 15, No. 12, December 2018, p. 615 - 623

ELECTRICAL AND OPTICAL PROPERTIES OF P-TYPE $Ag_{0.3}Cu_{0.7}InQ_2$ CHALCOPYRITE SEMICONDUCTORS

S. MORIS[a], V. MANRÍQUEZ[b], P. BARAHONA[c], A. GALDÁMEZ[b], P. VALENCIA-GÁLVEZ[b,*]

[a]*Vicerrectoría de Investigación y postgrado, Universidad Católica del Maule, Avenida San Miguel 3605, Talca 3480112, Chile*

[b]*Facultad de Ciencias, Departamento de Química, Universidad de Chile, Las Palmeras 3425, Santiago, 7800003 Chile*

[c]*Facultad de Ciencias Básicas, Universidad Católica del Maule, Avenida San Miguel 3605, Talca 3480112, Chile*

We report the synthesis, characterization and electrical properties of $Ag_{0.3}Cu_{0.7}InS_2$, $Ag_{0.3}Cu_{0.7}InSe_2$ and $Ag_{0.3}Cu_{0.7}InTe_2$. These solid solutions were synthesized *via* microwave-assisted solid-state reactions. Powder X-ray diffraction patterns were indexed in the space group $I\bar{4}2d$. The chemical compositions were determined by scanning electron microcopy. The analysis of the vibrational properties was performed by Raman scattering measurements. The Raman peaks were analyzed by fitting the spectra and allowed the identification of the vibrational modes *via* comparison with experimental and theoretical data from $CuInQ_2$ (Q = S, Se, Te) end-members. $Ag_{0.3}Cu_{0.7}InS_2$ and $Ag_{0.3}Cu_{0.7}InTe_2$ exhibit typical semiconductor *p*-type behavior with a carrier concentration of ~ $+10^{16}$ cm^{-3}. The electrical conductivities σ at R.T. were ~10^{-1} S cm^{-1} and ~1.0 S cm^{-1} for $Ag_{0.3}Cu_{0.7}InS_2$ and $Ag_{0.3}Cu_{0.7}InTe_2$, respectively. The optical band gaps, based on the UV-Vis-NIR spectra, were E_g ~1.50 eV.

(Received October 31, 2018; Accepted December 7, 2018)

Keywords: Semiconductor compound, p-Type, chalcopyrite-type

1. Introduction

During recent decades many researchers have studied and optimized the electrical properties of photovoltaic systems. The results have been obtained on heterojunction thin film devices, where the best efficiencies have been achieved using absorbent materials with band gaps of approximately 1.5 eV[1]. To achieve the above results, research has focused on optimizing photovoltaic conversion by improving the fundamental parameters; the fundamental parameters include the band gap of the semiconductor and the stoichiometric composition, which allows control of the structural, electrical and optical properties of the absorbent material.

The study of semiconductors based on type AMQ_2 metal chalcogenides is of great interest for their applications in optoelectronic devices and photovoltaic systems[1]–[4]. In particular, these compounds show characteristics that are interesting, such as high absorption coefficients, excellent coverage of the solar spectrum and high stability against solar irradiation. Among the most studied materials of this family are ternary compounds, $CuInQ_2$, $CuAlQ_2$ (Q = S, Se and Te)[4]–[11]; $CuMTe_2$ (M = Al, Ga and In)[12] and $AgInS_2$[13]–[17], which have been used as solar absorbers in photovoltaic cells. However, despite the attractive characteristics of ternary semiconductors, they generally have a relatively low efficiency. Nevertheless, band-gap, absorption coefficient and conversion efficiency can be improved by chemical substitutions that allow the synthesis of quaternary semiconductors. For example, the quaternary compound, $Cu(In_{1-x}Ga_x)Se_2$ (CIGSe), achieves significantly higher efficiencies of greater than 20%[18]–[23]; However, a Ga/(In + Ga) stoichiometric ratio of approximately 0.3 (an increase in the content of gallium) degrades the electronic properties of CIGSe[18], [20], [21]. The stoichiometry directly

* Corresponding author: p.valencia.galvez@gmail.com

modifies the electrical properties, because slight changes in the molar ratios between A/M and A/Q ratios give rise to changes in the resistivity, optical gap and carriers. We are interested in studying the effect of partial, isomorphic and isoelectronic substitution of copper for silver in copper-indium-Q ternary semiconductors (Q = S, Se and Te). This compound is used due to its high efficiency and that its crystalline structure (chalcopyrite type) remains isomorphic by partially substitution for a range of appropriate catonic radii, among other properties.

Previously, several methods have been reported for the synthesis of these type of compounds, including sputtering, electrodeposition, chemical vapor deposition and solvo-thermal methods [24]–[29]. However, the search for simple, fast and highly efficient methods to synthesize this type of material remains important. A very good alternative is microwave-assisted synthesis, [2], [30]–[33] this methodology has the benefits of selective, uniform and volumetric heating, rapid energy supply, high reaction yields, and clean reactions of the by-products[31], [32]. Additionally, it is emphasized that it is possible to perform reactions under solvent-free conditions, instead of using a solid support, such as alumina (basic or neutral), silica, or montmorillonite.

In this paper, we report the synthesis, structural, vibrational characterization, optical and electrical properties of the solid solutions $Ag_{0.3}Cu_{0.7}InS_2$, $Ag_{0.3}Cu_{0.7}InSe_2$ and $Ag_{0.3}Cu_{0.7}InTe_2$ that were synthesized by assisted solid-state reactions using microwaves. The aim of this research is to study the influence of the chemical substitution of 30% silver in the copper sites. Moreover, this isovalent substitution of the metal influences the band structure of the solid solutions, and the nature of the chalcogenides for each phase is different. In this work, it was possible to successfully obtain new compounds where energy of the band-gap approaches 1.5 eV, a value that better matches with the maximum conversion of the solar spectrum for a photovoltaic device.

2. Experimental section

2.1. Synthesis

$Ag_{0.3}Cu_{0.7}InS_2$, $Ag_{0.3}Cu_{0.7}InSe_2$ and $Ag_{0.3}Cu_{0.7}InTe_2$ were synthesized by direct combination of metal powders in stoichiometric amounts under microwave irradiation. The stoichiometric mixtures of the starting reagents ―Ag (powder 99.99%, Aldrich), Cu (powder 99.9+%, Aldrich), In (powder 99.99%, Aldrich), Se (powder 99.99+%, Aldrich), S (powder 99.5%, Aldrich) and Te (powder 99.9%, Aldrich) ― were placed into dried quartz tubes under an argon atmosphere. The tubes were evacuated and flame-sealed under an argon atmosphere. The syntheses were carried out with a microwave oven (HL25G, Howland) of frequency 2.45 GHz and a power of 850 Watt, with working time of 3 minutes of exposure[33].

2.2. Powder X-ray diffraction measurements

Powder X-ray diffraction patterns were collected at room temperature on a Bruker D8 Advance powder diffractometer (CuKα radiation, λ = 1.54098 Å) operating at 40 kV and 25 mA, in the range $5° < 2\theta < 80°$. The XRD patterns were indexed using the software CHECKCELL.

2.3. SEM-EDS analysis

The chemical compositions of the samples were determined by scanning electron microscopy (SEM) using a Vega 3 Tescan with Bruker Quantax 400 energy dispersive X-ray spectroscopy (EDS) detectors. The analysis was performed on the compressed samples, and multiple distinct areas were analyzed on each sample.

2.4. Raman scattering measurements

The Raman scattering measurements were performed using a RM1000 Renishaw micro-Raman spectrometer with CCD detectors in combination with a Leica LM/PM microscope using a 514 nm wavelength excitation. The spectrometer was calibrated using a reference single-crystal Si sample (Raman peak at 520.7 cm^{-1}). The spectral data were collected at room temperature in the backscattering configuration in the spectral range of 100-400 cm^{-1} with a laser spot on the sample of approximately 1 μm and a laser power of 2 mW.

2.5. Diffuse reflectance measurements

Diffuse reflectance spectra were recorded on an Agilent Technologies, Cary Series UV-Vis-NIR spectrophotometer, model Cary 5000 UV-Vis-NIR. The measurements were carried out between 500 and 1600 nm using microcrystalline samples, directly dispersed onto the sample holder.

2.6. Electrical properties

Hall-effect measurements were performed with an ECOPIA HMS 2000 equipment. The pellets for electrical measurements were uniaxially pressed at ~ 2.5 tons, resulting in cylindrical pellets with a 9.00 mm diameter and a thickness ranging from 0.93 to 1.30 mm. Then, the samples were sintered for 36 h at 550°C. The Hall coefficient, ±0.556 T, was obtained from the linear fit of the Hall resistivity. The electrical conductivity was measured by the Van der Pauw method from room temperature (R.T.) to 400 K. The gold electrical contacts on the pellets were deposited by sputtering. The density (ρ) was determined using the dimensions and mass of the sample, corresponding to an average pellet density of ~92% (experimental density/crystallographic density).

3. Results and discussion

3.1. Compositional characterization and X-ray powder diffraction

The chemical compositions were confirmed by SEM-EDS analyses (Fig. 1). The microprobe analysis EDS of several areas of the samples showed an average chemical substitution of copper by silver of 30% (Table 1).

The Fig. 2 shows the powder X-ray diffraction (PXRD) patterns were indexed in the $I\bar{4}2d$ space group. The $Ag_xCu_{1-x}InQ_2$ (Q = S, Se, Te) phases have the chalcopyrite-type crystal structure in which the copper crystallographic positions (Wyckoff site 4a) are occupied randomly by silver and copper atoms. As expected, the indexed diffraction peaks of $Ag_{0.3}Cu_{0.7}InSe_2$ and $Ag_{0.3}Cu_{0.7}InTe_2$ show a shift of the reflection positions towards lower values of 2θ, with respect to those from $Ag_{0.3}Cu_{0.7}InS_2$; this is attributed to the size of tellurium and selenium atoms, which are larger than sulfur atoms. The substitution of Cu^+ cations (radius ~0.98 Å) by Ag^+ cations (radius ~1.28 Å) leads to an increase of the cell volume (Table 2). Robbins *et al.*[34] have suggested that the crystalline structure of the chalcopyrite undergoes a deformation of the tetrahedral coordination, which can be measured through the δ coefficient (see Table 2). The coefficient δ depends on the difference between the average A-A and M-M interactions compared to A-M interactions. The δ values show that the chemical substitution of silver by copper does not substantially affect the chalcopyrite-type crystal structure.

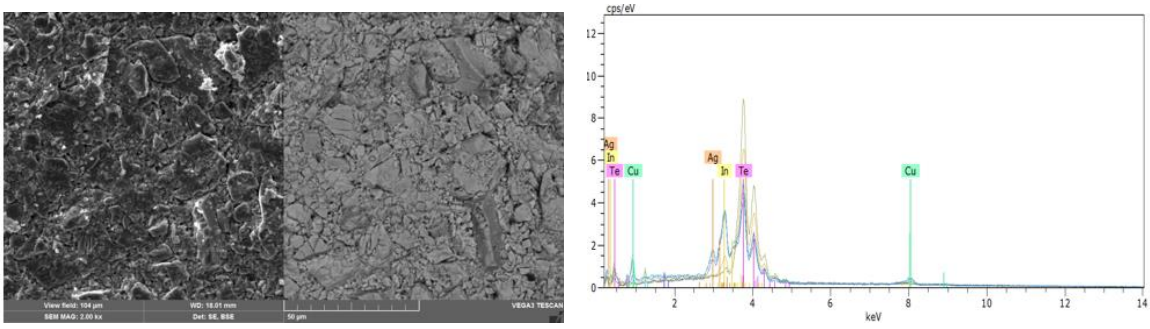

Fig. 1. Image of secondary electrons and backscattered of the phase $Ag_{0.3}Cu_{0.7}InTe_2$ (left) and EDS spectrum of the polycrystalline material (right).

Table 1. Chemical compositions of the samples $Ag_{0.3}Cu_{0.7}InQ_2$ (Q = S, Se, Te) determined by EDS.

Samples	Mass (%)				Experimental
	Ag	Cu	In	Q	
$Ag_{0.3}Cu_{0.7}InS_2$	16.12	15.42	43.54	24.92	$Ag_{0.39}Cu_{0.64}In_{1.00}S_{2.05}$
$Ag_{0.3}Cu_{0.7}InSe_2$	9.21	12.43	33.36	45.33	$Ag_{0.29}Cu_{0.67}In_{1.00}Se_{1.98}$
$Ag_{0.3}Cu_{0.7}InTe_2$	6.83	10.67	26.79	55.53	$Ag_{0.27}Cu_{0.72}In_{1.00}Te_{1.87}$

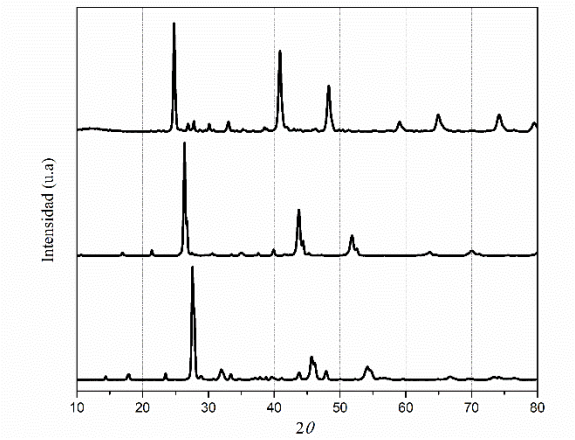

Fig. 2. XRD powder pattern of the product from microwave synthesis $Ag_{0.3}Cu_{0.7}InS_2$ (bottom), $Ag_{0.3}Cu_{0.7}InSe_2$ (middle) and $Ag_{0.3}Cu_{0.7}InTe_2$ (top).

Table 2. Lattice parameters and tetragonal distortion data determined for the phases $Ag_{0.3}Cu_{0.7}InQ_2$ and that reported for the ternary end-members $CuInQ_2$ and $AgInQ_2$ (Q = S, Se, Te).

Samples	V(Å)	c/a	δ*
$CuInS_2$	330.01	2.026	-0.0026
$Ag_{0.3}Cu_{0.7}InS_2$	350.84 (0.02)	1.978	0.0222
$AgInS_2$	371.99	1.89	0.11
$CuInSe_2$	385.67	2.01	-0.01
$Ag_{0.3}Cu_{0.7}InSe_2$	401.40 (0.03)	1.9766	0.0234
$AgInSe_2$	450.75	1.941	0.059
$CuInTe_2$	469.09	2.00	0.00
$Ag_{0.3}Cu_{0.7}InTe_2$	493.37 (0.01)	2.0030	-0.0030
$AgInTe_2$	505.73	2.060	-0.060

*δ =2-c/a

3.2. Raman scattering analysis

A detailed study of the Raman spectrum of the chalcopyrite $CuInSe_2$ was reported by Rincón *et al.* [35]. From a vibrational point of view, the representation of the optical phonon modes in the chalcopyrite-type crystal structure can be written as Γ: $A1 \oplus 2A2 \oplus 3B1 \oplus 4B2 \oplus 7E$ [35].

Fig. 3 shows the Raman spectra for $Ag_{0.3}Cu_{0.7}InS_2$, $Ag_{0.3}Cu_{0.7}InSe_2$ and $Ag_{0.3}Cu_{0.7}InTe_2$ fitted with Lorentzian curves in the range 100-400 cm^{-1}, where the main spectral changes occur.

The principal Raman line in chalcopyrite-type AMQ_2 (Q = S, Se and Te) is the vibrational mode *A1*, which involves Q-atoms displacements (breading mode) [13, 14]. Table 3 summarizes the frequency determined for mode *A1* for the solid solutions synthesized in this work, together with those reported for ternary chalcogenide end-members.

Interestingly, the mode *A1* frequencies in the $Ag_{0.3}Cu_{0.7}InQ_2$ phase are systematically lower than that in the corresponding end-member, $CuInQ_2$. The inverse trend is observed with respect to $AgInQ_2$, where mode *A1* in $Ag_{0.3}Cu_{0.7}InQ_2$ is always slightly higher. However, in both cases, the difference decreases with the increasing atomic weight of Q. Further Raman emissions that were observed at lower frequencies, ~128 cm^{-1} and ~126 cm^{-1}, correspond to $Ag_{0.3}Cu_{0.7}InS_2$ and $Ag_{0.3}Cu_{0.7}InSe_2$, respectively. The Raman spectrum of the $Ag_{0.3}Cu_{0.7}InQ_2$ solid solutions show relatively weak peaks at ~323, 217 and 138 cm^{-1} for $Ag_{0.3}Cu_{0.7}InS_2$, $Ag_{0.3}Cu_{0.7}InSe_2$ and $Ag_{0.3}Cu_{0.7}InTe_2$, respectively, which may be assigned to the *B2* and *E* vibration modes detected in the ternary and quaternary chalcopyrite-derivatives[11], [25], [27], [28], [35], [36], [37].

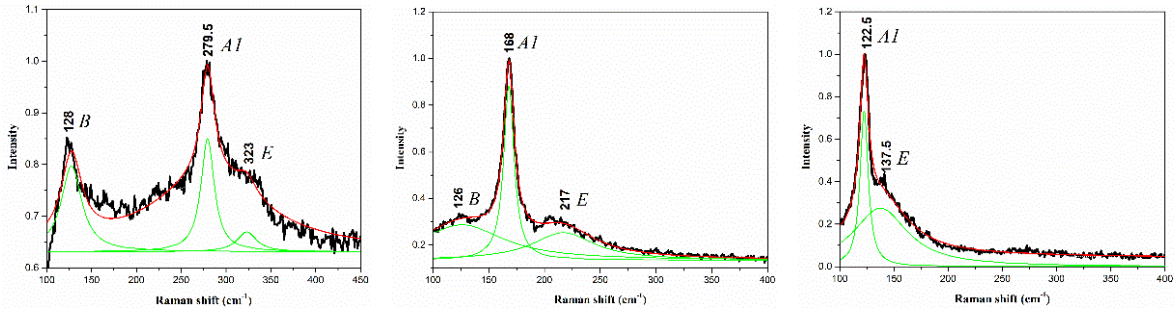

Fig. 3. Raman spectrum of samples $Ag_{0.3}Cu_{0.7}InS_2$ (left), $Ag_{0.3}Cu_{0.7}InSe_2$ (middle) and $Ag_{0.3}Cu_{0.7}InTe_2$ (right) with the different contributions as deduced from the fitting of the different peaks with Lorentzian (Green lines).

Table 3. Wavenumbers of A_1 Raman modes of different Cu-, Ag- and $Ag_{0.3}Cu_{0.7}InQ_2$ (Q = S, Se, Te) – chalcopyrites.

Phases	Wavenumber (cm^{-1})	References
$CuInS_2$	290	[6], [8]
$Ag_{0.3}Cu_{0.7}InS_2$	279.5	*
$AgInS_2$	265	[29]
$CuInSe_2$	173	[6], [8]
$Ag_{0.3}Cu_{0.7}InSe_2$	168	*
$AgInSe_2$	172	[29]
$CuInTe_2$	125	[30]
$Ag_{0.3}Cu_{0.7}InTe_2$	122.5	*
$AgInTe_2$	122	[31]

* This work

3.3. Optical properties

Reflectance spectra for $Ag_{0.3}Cu_{0.7}InQ_2$ were determined in the range of 500-1600 nm. The optical band gap E_g was calculated using the Tauc relationship (eqn. 1) [38], where α is the absorption coefficient of the material, A is a constant, hν is the incident photon energy and E_g is the band gap.

$$\alpha h\nu = A\,(h\nu - E_g)^n \quad (1)$$

The characteristic value of n=½, corresponding to semiconductors with direct band transitions (VB to CB), was used for the materials that were synthesized in this work. The calculation of E_g according to (Eq. 1) from the linear fit of $(\alpha h\nu)^2$ vs. hν is shown in Fig. 4. The E_g

values for $Ag_{0.3}Cu_{0.7}InS_2$, $Ag_{0.3}Cu_{0.7}InSe_2$ and $Ag_{0.3}Cu_{0.7}InTe_2$ were 1.54, 1.53 and 1.47 eV, respectively. These values are very interesting because a theoretical conversion efficiency in single-junction cells that was close to 30% was obtained for solar cells with an absorbent material that had a band gap of ~1.5 eV [13]. These results have drawn attention because we expected that the substituted chalcogen would cause an increased bandwidth of the conduction band and therefore a decrease in the band gap of $Ag_{0.3}Cu_{0.7}InQ_2$ that was synthesized by replacing sulfur by selenium and then selenium by tellurium. This assumption was based on the work reported by Hussain et *al.*[39] and Xian-Zhou et *al.* [12]. Hussain et *al.* performed calculations of the band-structure for $CuAlQ_2$ compounds (Q = S, Se, Te) using the FP-LAPW method. Their results showed that these compounds have similar band-structures with a direct gap and a bandwidth that decreases when the sulfur is replaced by selenium and then the selenium is replaced by tellurium. The authors attribute these effects to the increase of the bandwidth of the conduction band due to the replacement of the group VI element. Additionally, Xian-Zhou et *al.* reported a theoretical study of the electronic structure and optical properties of the $CuMTe_2$ (M = Al, Ga, In) compounds. The results for these semiconductors showed a similar behavior to that reported by Hussain et *al.*; the forbidden bandwidth decreases, depending on the element replaced, according to the following order: aluminum (Al), gallium (Ga) and indium (In). However, our compound does not exhibit this behavior. These differences in the results are attributed to the chemical substitutions of copper by silver, which would also generate a new distribution of defects in the network, corresponding to ordered vacancies of copper (Vcu^+). According to several theoretical calculations, the d-orbital of the copper forms an anti-entanglement state with the orbital p of the Q atoms, which is responsible for the energy level that determines the maximum of the valence band [16] - [19]. Wasim et *al.*[40] observed this behavior in $CuInSe_2$ and $CuInTe_2$ chalcopyrite, where a decrease in copper leads to a pronounced downward displacement of the maximum of the valence band, whereas the minimum of the conduction band remains at approximately the same energy level.

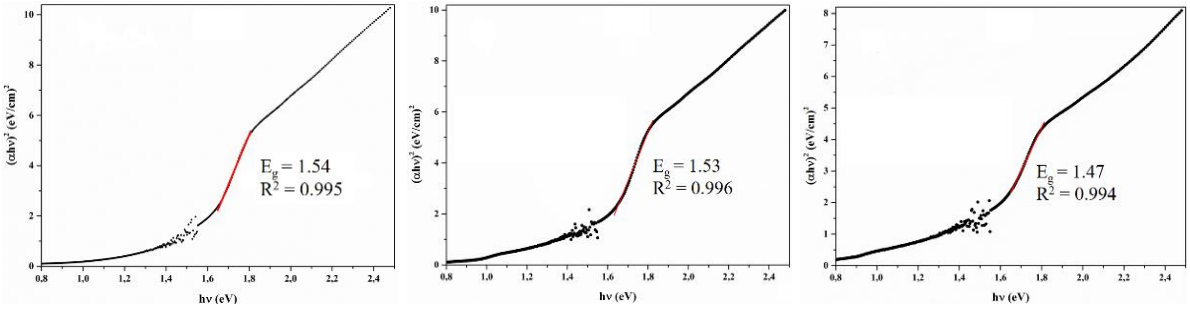

Fig. 4. Plot of $(\alpha h\nu)^2$ against photon energy (hv) for samples $Ag_{0.3}Cu_{0.7}InS_2$ (left), $Ag_{0.3}Cu_{0.7}InSe_2$ (middle) and $Ag_{0.3}Cu_{0.7}InTe_2$ (right).

3.4. Electrical properties

The electrical characterizations of $Ag_{0.3}Cu_{0.7}InS_2$ and $Ag_{0.3}Cu_{0.7}InTe_2$ were carried out by the Hall effect and Van der Pauw method (carrier concentration and mobility) [41]. Figure 5 shows the temperature dependence of conductivity (σ). There is a monotonic increase of σ with increasing temperature, which indicates a typical semiconductor behavior. This dependence has been well described by the following exponential equation [6], [18]:

$$\sigma(T) = \sigma_0 e^{-Ea/kT} \quad (2)$$

The linear fit of lnσ vs 1000/T shows the typical Arrhenius behavior, which indicates that the electrical transport is thermally active. The activation energies for $Ag_{0.3}Cu_{0.7}InS_2$ and $Ag_{0.3}Cu_{0.7}InTe_2$ were 0.199 and 0.265 eV, respectively. These values are lower compared to the values reported for ternary phase $CuInQ_2$ (Q = S, Se, Te) end-members [6]. This behavior may be caused by the increased density of acceptor impurities due to the replacement of silver by copper in the compounds [42].

The Hall coefficients are positive in the temperature range from 298 to 403 K, which is indicative of p-type conductivity. Figures 6 and 7 shows the hole concentrations N_p and the mobility as a function of temperature, respectively. The hole mobility is not particularly high: approximately 7.0-20 cm^2 V^{-1} S^{-1} for $Ag_{0.3}Cu_{0.7}InTe_2$ and 35-40 cm^2 V^{-1} S^{-1} for $Ag_{0.3}Cu_{0.7}InS_2$. This result is consistent with the behavior previously reported by Abo et *al.* [6]. The value of N_p increases approximately linearly with increasing temperature, following a temperature dependence of $N_p \sim T^n$. However, the carrier concentrations were relatively low, approximately ~+10^{16} cm^{-3} at room temperature in $Ag_{0.3}Cu_{0.7}InTe_2$, which also showed lower conductivity and mobility. The carrier concentration of $CuInTe_2$ were on the order of ~+10^{18} cm^{-3} at 300 K[43]. Breck et *al.* suggested that to increases the efficiency of CGS-based devices it is necessary to reduce the carrier concentration of the absorber[44]. The carrier concentration decrease in $Ag_{0.3}Cu_{0.7}InTe_2$ and $Ag_{0.3}Cu_{0.7}InS_2$ may be associated with the defect modifications due to the chemical substitution of Ag by Cu atoms. Stephan et *al.* reported experimental correlation between stoichiometry and native point defects in the chalcopyrite ternary compound $CuInSe_2$[45]. The neutron powder diffraction experimental results show that Cu vacancies (V_{Cu}) cause *p*-type conductivity. These defects are correlated with the Cu/In molar ratio (nonstoichiometry). The reductions of carrier concentration from ~+10^{18} cm^{-3} to ~+10^{16} cm^{-3} could be attributed to a decrease of V_{Cu} due to the substitution of 30% in the copper sites by Ag atoms.

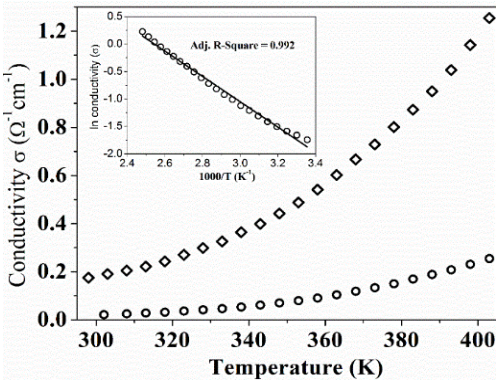

Fig. 5. Plot of electrical conductivity (σ) versus temperature, for $Ag_{0.3}Cu_{0.7}InS_2$ (squares) and $Ag_{0.3}Cu_{0.7}InTe_2$ (circles). The Insert show lnσ vs 1000/T, for $Ag_{0.3}Cu_{0.7}InTe_2$ phase.

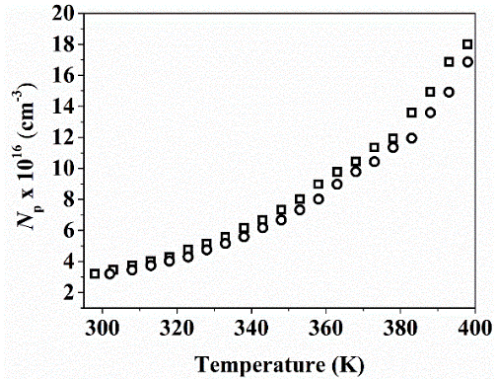

Fig. 6. Plot of carriers (Np) as a function of temperature, of the solid solutions $Ag_{0.3}Cu_{0.7}InS_2$ (squares) and $Ag_{0.3}Cu_{0.7}InTe_2$ (circles).

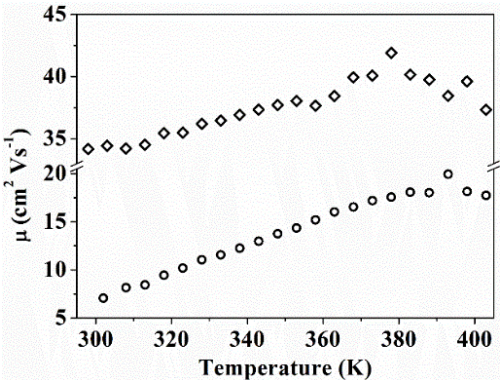

Fig. 7. Plot of carrier mobility (μ) as a function of temperature, of the solid solutions $Ag_{0.3}Cu_{0.7}InS_2$ (squares) and $Ag_{0.3}Cu_{0.7}InTe_2$ (circles).

4. Conclusions

$Ag_{0.3}Cu_{0.7}InS_2$, $Ag_{0.3}Cu_{0.7}InSe_2$ and $Ag_{0.3}Cu_{0.7}InTe_2$ were successfully synthesized *via* microwave-assisted solidstate reactions. These phases belong to the space group $I\bar{4}2d$ (chalcopyrite-type), the Raman spectra allowed us to confirm that we are in the presence of the quaternary phase showing the characteristic peaks and displacements for this type of structure. $Ag_{0.3}Cu_{0.7}InS_2$ and $Ag_{0.3}Cu_{0.7}InTe_2$ exhibit typical semiconductor *p*-type behavior with a carrier concentration of approximately ~ $+10^{16}$ cm^{-3}.

These results could be attributed to a decrease of V_{Cu} due to the random substitutions of Cu by Ag atoms. The latter is a promising result because is obtained products the excellent quality be used as energy absorbers in solar cells.

Acknowledgments

The authors thank the financial support of FONDECYT Post-doctoral project 3140512 and the Chilean-French International Associated Laboratory for "Multifunctional Molecules and Materials" (LIAM3-CNRS N°1027).

References

[1] D. Aldakov, A. Lefrançois, P. Reiss, J. Mater. Chem. C **1**, 3756 (2013).
[2] C. Landry, R. Barron, Science **260**(5114), 1653 (1993).
[3] J. Müller, J. Nowoczin, H. Schmitt, Thin Solid Films **496**(2), 364 (2006**)**.
[4] S. R. Kodigala, Thin Films and Nanostruc. **35**, 319 (2010).
[5] T. Ryo, D. Nguyen, M. Nakagiri, N. Toyoda, H. Matsuyoshi, S. Ito, Thin Solid Films **519**(21), 7184 (2011).
[6] A. M. Abo El Soud, H. A. Zayed, L. I. Soliman, Thin Solid Films **229**, 232 (1993).
[7] J. Zhou, S. Li, X. Gong, Y. Yang, L. You, Y. Guo, Mater. Lett. **65**(23-24), 3465 (2011).
[8] J. Liu, J. Li, G. Jiang, W. Liu, C. Zhu, Mater. Lett. **156**, 153 (2015).
[9] S. M. Hosseinpour-Mashkani, M. Salavati-Niasari, F. Mohandes, K. Venkateswara-Rao, Mater. Sci. Semicond. Process. **16**, 390 (2013).
[10] J. Bernède, L. Assmann, Vacuum **59**(4), 885 (2000).
[11] C. Rincon, S. Wasim, G. Marin, E. Hernandez, J. Delgado, J. Galibert, G. Marin, J. Appl. Phys. **88**(6), 3439 (2000).
[12] X. Z. Zhang, K. S. Shen, Z. Y. Jiao, X. F. Huang, Comput. Theor. Chem. **1010**, 67 (2013).
[13] W. Zhang, D. Li, Z. Chen, M. Sun, W. Li, Q. Lin, X. Fu, Mater. Res. Bull. **46**(7),

975 (2011).
[14] A. Tadjarodi, A. H. Cheshmekhavar, M. Imani, Appl. Surf. Sci. **263**, 449 (2012).
[15] W. Xiang, C. Xie, J. Wang, J. Zhong, X. Liang, H. Yang, L. Luo, Z. Chen, J. Alloys. Comp. **588**, 114 (2014**)**.
[16] M. Mousavi-Kamazani, M. Salavati-Niasari, Compos. Part B: Eng. **56**, 490 (2014).
[17] L. Borkovska, A. Romanyuk, V. Strelchuk, Y. Polishchuk, V. Kladko, A. Raevskaya, O. Stroyuk, T. Kryshtab, Mater. Sci. Semicond. Process. **37**, 135 (2015).
[18] R. Caballero, C. Guillen, Thin Solid Films **431**(3), 200 (2003).
[19] M. Panthani, V. Akhavan, B. Goodfellow, J. P. Schmidtke, L. Dunn, A. Dodabalapur, P. F. Barbara, B. A. Korgel, J. Am. Chem. Soc. **130**(49), 16770 (2008).
[20] U. P. Singh, Vacuum **83**(11), 1344 (2009).
[21] Y. Wang, Z. Jin, H. Liu, X. Wang, X. Zheng, H. Du, Powder Technol. **232**, 93 (2012).
[22] J. F. Han, C. Liao, E. Gautron, T. Jiang, H. M. Xie, K. Zhao, M. P. Besland, Vacuum **105**, 46 (2014**)**.
[23] G. Li, W. Liu, Y. Liu, S. Lin, Y. Zhang, Z. Zhou, Q. He, Y. Sun, Sol. Energy Mater. Sol. Cells **139**, 108 (2015).
[24] W.-H. Hsu, H.-I. Hsiang, S. Yu, Ceram. Int. **41**(2), 3208 (2015).
[25] M. Berruet, M. Valdes, S. Cere, M. Vazquez, J. Mater. Sci. **47**(5), 2454 (2012**)**.
[26] R. Scheer, A. Perez-Rodriguez, W. Metzger, Prog. Photovolt. **18**(6), 467 (2010).
[27] A. Tverjanovich, S. Bereznev, Scientific Journal of Riga Tecchnical University Material Science and Applied Chemistry. **21**, 79 (2010**)**.
[28] C. Insignares-Cuello, C. Broussillou, V. Bermúdez, E. Saucedo, a. Pérez-Rodríguez, V. Izquierdo-Roca, Appl. Phys. Lett. **105**(2), 21905 (2014).
[29] J. López-García, M. Placidi, X. Fontané, V. Izquierdo-Roca, M. Espindola, E. Saucedo, C. Guillén, J. Herrero, A. Pérez-Rodriguez, Sol. Energy Mater. Sol. Cells **132**, 245 (2015).
[30] C. C. Landry, J. Lockwood, A. R. Barron, Chem. Mater. **7**, 699 (1995).
[31] K. J. Rao, B. Vaidhyanathan, M. Ganguli, P. Ramakrishnan, Chem. Mater. **11**, 882 (1999).
[32] S. Chandrasekaran, T. Basak, S. Ramanathan, J. Mater. Process. Technol. **211**(3), 482 (2011).
[33] P. Valencia-Gálvez, G. Galdámez, V. Manríquez, G. González, Chalcogenide Lett. **13**(5), 207 (2016).
[34] M. Robbins, J. C. Phillips, B. Laboratories, J. Phys Chem. Solid. **34**, 1205 (1973).
[35] C. Rincón, F. J. Ramírez, *J. App. Phys.* **72**(9), 4321 (1992).
[36] C. Insignares-Cuello, V. Izquierdo-Roca, J. López-García, L. Calvo-Barrio, E. Saucedo, S. Kretzschmar, T. Unold, C. Broussillou, T. Goislard de Monsabert, V. Bermudez, A. Pérez-Rodríguez, Sol. Energy **103**, 89 (2014).
[37] K. R. Murali, P. Muthusamy, A. Panneerselvam, J. Mater. Sci.: Mater. Electron. **24**, 3412 (2013).
[38] A. M. J. Tauc, J. Non-Crystal. Solids **8-10**, 569 (1972).
[39] A. H. Reshak, S. Auluck, Solid State Comm. **145**(11-12), 571 (2008).
[40] S. M. Wasim, C. Rincón, G. Marín, J. M. Delgado, Appl. Phys. Lett. **77**(1), 94 (2000).
[41] L. J. van den Pauw, Philips Tech. Rev. **20**, 220 (1958).
[42] C. Persson, A. Zunger, App. Phys. Lett. **87**(21), 1 (2005).
[43] R. Liu, L. Xi, H. Liu, X. Shi, W. Zhang, L. Chen, Chem. Comm. **48**(32), 3818 (2012).
[44] X. X. Liu, J. R. Sites, J. App. Phys. **75**(1), 577 (1994).
[45] C. Stephan, S. Schorr, M. Tovar, H. W. Schock, App. Phys. Lett. **98**(9), 10 (2011).